Structure-directed discovery of potent non-peptidic inhibitors of human urokinase that access a novel binding subsite

Vicki L Nienaber[1]*, Donald Davidson[2], Rohinton Edalji[1], Vincent L Giranda[2], Vered Klinghofer[2], Jack Henkin[2], Peter Magdalinos[1], Robert Mantei[2], Sean Merrick[1], Jean M Severin[1], Richard A Smith[1], Kent Stewart[1], Karl Walter[1], Jieyi Wang[2], Michael Wendt[2], Moshe Weitzberg[2], Xumiao Zhao[2] and Todd Rockway[2]*

Background: Human urokinase-type plasminogen activator has been implicated in the regulation and control of basement membrane and interstitial protein degradation. Because of its role in tissue remodeling, urokinase is a central player in the disease progression of cancer, making it an attractive target for design of an anticancer clinical agent. Few urokinase inhibitors have been described, which suggests that discovery of such a compound is in the early stages. Towards integrating structural data into this process, a new human urokinase crystal form amenable to structure-based drug design has been used to discover potent urokinase inhibitors.

Results: On the basis of crystallographic data, 2-naphthamidine was chosen as the lead scaffold for structure-directed optimization. This co-crystal structure shows the compound binding at the primary specificity pocket of the trypsin-like protease and at a novel binding subsite that is accessible from the 8-position of 2-napthamidine. This novel subsite was characterized and used to design two compounds with very different 8-substituents that inhibit urokinase with K_i values of 30–40 nM.

Conclusions: Utilization of a novel subsite yielded two potent urokinase inhibitors even though this site has not been widely used in inhibitor optimization with other trypsin-like proteases, such as those reported for thrombin or factor Xa. The extensive binding pockets present at the substrate-binding groove of these other proteins are blocked by unique insertion loops in urokinase, thus necessitating the utilization of additional binding subsites. Successful implementation of this strategy and characterization of the novel site provides a significant step towards the discovery of an anticancer clinical agent.

Addresses: [1]Department of Structural Biology, Abbott Laboratories, Abbott Park, IL 60064-6098, USA and [2]Department of Cancer Research, Abbott Laboratories, Abbott Park, IL 60064-6098, USA.

*Corresponding authors.
E-mail: vicki.nienaber@abbott.com
todd.rockway@abbott.com

Key words: drug design, inhibitors, tumor metastasis, urokinase, X-ray crystallography

Received: 20 December 1999
Revisions requested: 10 February 2000
Revisions received: 29 February 2000
Accepted: 2 March 2000

Published: 3 May 2000

Structure 2000, 8:553–563

0969-2126/00/$ – see front matter

Introduction

Urokinase, a trypsin-like serine protease, degrades basement membranes and interstitial matrices via a cascade mechanism involving plasminogen and metalloproteases [1–3]. This tissue remodeling is part of the disease progression in cancer, arthritis [4,5], atherosclerosis [6,7], and post-myocardial infarction heart rupture [8]. Cancer invasion and metastasis are the primary causes of mortality and morbidity of malignancy [9]. In order to take effect, invasion and metastasis require the degradation of basement membranes and other extracellular protein structures. High levels of urokinase activity are associated with many cancers, and furthermore, increased urokinase activity is an independent predictor of the diseased state [10]. Tumors invade and metastasize more slowly in urokinase-knockout mice than they do in control animals [11]. Inhibitors of urokinase have been reported to slow tumor metastasis and the growth of the primary tumor [12–16]. These data suggest that inhibition of urokinase activity might retard the progression of cancer in humans.

In addition to urokinase enzymatic activity, other components of the urokinase–plasminogen pathway have also been implicated in the growth and invasion of tumors. The N-terminal growth-factor-like domain of urokinase binds to its cellular receptor urokinase-type plasminogen activator receptor (uPAR). Inhibition of this interaction has been shown to diminish the growth of tumors in xenograft models [17,18]. Plasminogen activator inhibitors 1 and 2 (PAI1 and PAI2) have also been implicated in the progression of tumors. Although high levels of PAI2 have been associated with better prognosis in humans [19,20], high concentrations of PAI1 have, paradoxically, been show to be associated with poor prognosis and lack of tumor progression [21–25].

Despite the potential clinical significance of blocking urokinase activity, few urokinase inhibitors have been reported. A peptide that selects for urokinase over tissue plasminogen activator has been identified using phage display. This peptide was engineered into PAI1 providing a specific macromolecular serpin inhibitor [26]. Inhibitor binding in the substrate groove has been visualized in the reported crystal structure of Glu-Gly-Arg-chloromethylketone–urokinase [27]. In addition to these peptide-derived inhibitors, small-molecule inhibitors [28–32] have also been reported. These contain a positively charged group that is expected to bind in the primary binding pocket of urokinase. Although most compounds are reported to inhibit in the micromolar range, two amidine-containing series are submicromolar inhibitors of urokinase. Two compounds from one series, B428 and B623, inhibit urokinase with an IC_{50} of 370 nM and 70 nM, respectively [29,30], whereas in another series an analog of the thrombin inhibitor *N*-(4-toluene-sulphonyl)-DL-*p*-amidinophenyl-alanyl-piperidine (TAPAP) inhibits with a K_i of 410 nM [33]. Co-crystal structures in both series have been completed, B428 in complex with urokinase [34] and the TAPAP analog in complex with trypsin [33]. Both compounds bind at the S_1 pocket although the binding mode of the TAPAP analog to trypsin would be sterically blocked in urokinase [33]. This work provides an important starting point for the design of more potent urokinase inhibitors.

Although urokinase inhibitors and structural data are available, there is a lack of reports describing structure-directed optimization of urokinase inhibitors. This is despite the large amount of literature available describing drug-design programs for the structurally similar blood-clotting enzymes thrombin and factor Xa [35–38]. The role of urokinase in the mechanism of tumor metastasis indicates that structural and functional characterization of the urokinase active site and the discovery of more potent small-molecule inhibitors should provide a significant step towards obtaining an anticancer clinical agent. To achieve this step a new crystal form of human urokinase [34], that diffracts to high resolution and permits complex formation by the compound soaking method, has been used to determine co-crystal structures with a series of small-molecule noncovalent inhibitors. The process provided characterization of a novel binding subsite adjacent to the primary binding pocket and yielded two of the most potent urokinase inhibitors reported to date.

Results and discussion

Identification of binding pockets and subsites for structure-directed drug design

Examination of the urokinase substrate-binding groove reveals that, apart from the primary binding S_1 pocket, this site is relatively featureless when compared with other trypsin-like serine proteases (Figure 1). For this family of proteins, positively charged small-molecule inhibitors make a salt bridge with Asp189 in the S_1 pocket [39]. Serine proteases such as thrombin, factor Xa, or tissue plasminogen activator [27,40–42], however, also have other secondary binding sites at S_2 and/or S_4 of the substrate-binding groove [33,38]. In urokinase, the size of S_2 and S_4 is greatly reduced owing to a two-residue insertion at position 97 (chymotrypsin numbering system), which effectively blocks both sites (Figure 1). Thus, urokinase inhibitors require S_1 as the anchor site but depend upon smaller pockets and/or subsites on the surface of the enzyme for lead optimization.

A number of amidine-based urokinase inhibitors have been reported [43] including benzamidine (K_i = 1 mM), 5-amidino-indole (K_i = 131 μM) [28], benzo(b)thiophene-2-carboxamidine (IC_{50} = 3.7 μM, starting scaffold for B428) [29,30], and 2-naphthamidine (K_i = 5.5 μM) [31]. These inhibitors are expected to bind at S_1, as demonstrated by the co-crystal structure of B428–urokinase [34] and also because of their net positive charge. Of these scaffolds, benzo(b)thiophene-2-carboxamidine and 2-naphthamidine are the most potent and exhibit selectivity against tissue plasminogen activator and plasmin. This selectivity might

Figure 1

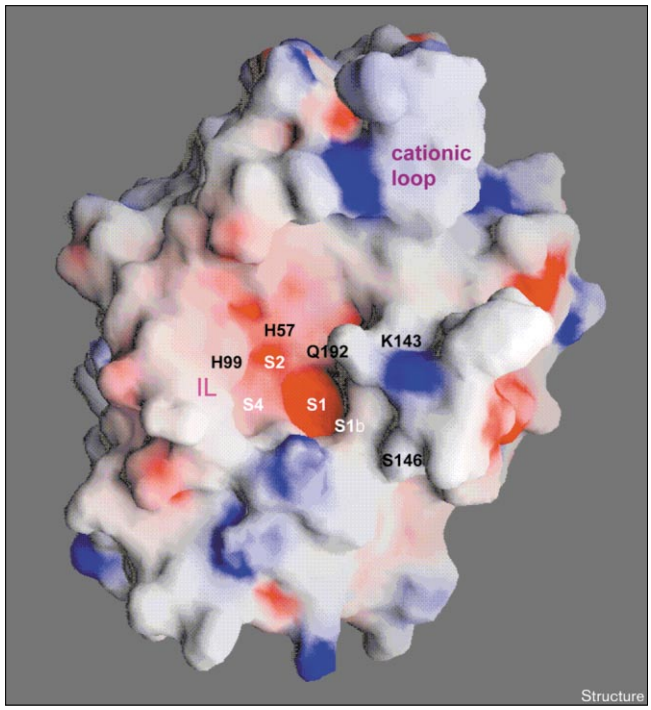

GRASP [58] surface representation of urokinase. Residues at the active site are labeled in black and binding residues within pockets in white. The substrate-binding groove consists of the S1, S2 and S4 pockets; the $S_{1\beta}$ subsite is directly adjacent to the substrate-binding groove. The insertion loop that partially obstructs S4 is labeled IL. The surface is colored according to electrostatic potential: red, negative; blue, positive.

Figure 2

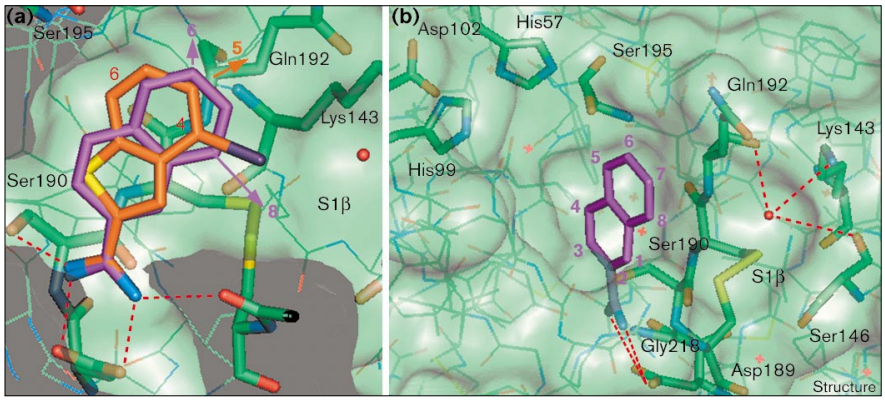

Crystal structures for choosing a starting scaffold. (**a**) Overlay of naphthamidine (purple) and B428 (orange) bound to urokinase showing a similar binding mode for the two amidine groups but different vectors toward the $S_{1\beta}$ pocket. Even though the naphthamidine 6-position and B428 5-position overlap, the vectors from these sites are very different. Partial numbering of the B428 (orange) and naphthamidine (purple) rings are also color coded. (**b**) Crystal structure of naphthamidine (purple) bound at the active site S_1 pocket of urokinase. Several residues participate in hydrogen bonds between the amidine group and protein (red dashed lines): Asp189 Oδ1 (3.1 Å), Ser190 Oγ (3.0 Å), Asp189 Oδ2 (2.9 Å) and Gly218 O (2.8 Å). Residues within the S_1 pocket that are in van der Waals contact with the inhibitor include Val213, Ser190 and Asp194 as well as the rim that consists of the Cys191–Cys220 disulfide bridge, and the mainchain atoms of Ser214–Cys220 and Gln192–Cys191. Hydrogen bonding between an ordered solvent molecule bound at $S_{1\beta}$ and the protein is also depicted (red dashed lines). Numbering of the naphthamidine ring system is shown in purple.

limit antifibrinolytic side effects *in vivo* [29–31]. To pick the best starting scaffold for structure-based drug design, the co-crystal structure for each scaffold bound to urokinase was examined and compared.

The crystal structure of 4-iodo benzo(b)thiophene-2-carboxamidine (B428) at 2.0 Å resolution [34] shows that the compound binds at S_1 (Figure 2a, orange) and that the inhibitor's 4-position is directed towards a novel subpocket termed $S_{1\beta}$ [34]. The $S_{1\beta}$ site is bounded by residues Gly218 and Ser146, the Cys191–Cys220 disulfide bridge, the sidechain of Lys143 and part of Gln192. In B428, the 4-iodo interacts at the entrance of $S_{1\beta}$ and results in an increase in potency from an IC_{50} of 3.7 μM to an IC_{50} of 0.320 μM [29,30], making this an attractive site for lead optimization. As reported previously [34], however, the 5- and 6-positions of B428 are less optimally situated for accessing other subpockets on the molecule (Figure 2a). More specifically, the substitution vector from the 5-position is directed towards Gln192 and out into the bulk solvent, whereas the 6-position is in close contact with Ser195 Oγ. The co-crystal structure of B428–urokinase reveals direct accessibility to the $S_{1\beta}$ site but not towards any other sites.

The co-crystal structure of 2-napthamidine urokinase (Figure 2b; Table 1) shows the inhibitor bound at the S_1 pocket. This is similar to the binding observed for substituted factor Xa naphthamidine inhibitors BM12.1700, BX5633 and/or DX-9065a when complexed with factor Xa, thrombin or trypsin [38,44,45]. In urokinase, the hydrogen bonding of the amidine nitrogens and the conformation of Asp189 is the same as observed for the thrombin and trypsin complex structures, and the naphthalene group is in van der Waals contact with the interior of the S_1 pocket. When naphthamidine inhibitors bind to factor Xa and thrombin a conformational shift of residues 191–193 by 1.5–2.0 Å is observed [38,44]; comparisons of naphtamidine-bound urokinase with the native protein show no such shift to occur.

Unlike B428, 2-naphthamidine presents more options for substitution. The naphthamidine 1-, 3- and 4-positions are in close contact with the protein and are therefore not open to further substitution (see ring-numbering system in Table 2 or Figure 2b). The 5-position points underneath the sidechain of Ser195 and might accommodate a small group, whereas the 6-, 7- and 8-positions might accommodate much larger substitutions. The 6-position points above S_2 and substitutions here are projected to interact with subsites above the peptide-binding groove. This is in contrast to the 6-position of B428 (Figure 2b), which is in close contact with Ser195 Oγ. The 7-position of 2-naphthamidine points towards Gln192 and bulk solvent and substitutions at this site will have limited interactions with urokinase. Naphthamidines with 7-substitutions such as compound **2** (Table 2) are, within error, equipotent to the parent compound. This is in contrast to the observation that 7-substituted naphthamidines are potent factor Xa inhibitors [38,44,45]. The 7-substituted factor Xa inhibitors use a second binding site at S_4 that is blocked and, therefore, not accessible in the urokinase structure. The 8-position of 2-napthamidine points towards the $S_{1\beta}$ pocket (Figure 2), which is an important site for binding in the benzo(b)thiophene-2-carboxamidine series of inhibitors [34]. No 8-substituted naphthamidine, however, has been reported as a trypsin-like protease inhibitor. Examination of the structural data, therefore, shows that both B428 and

Table 1

X-ray data and model statistics.

Data set	–H*	–NH_2*	–NHCOObenz*	–NHCOOMe*	–NHpyr*
Space group	$P2_12_12_1$	$P2_12_12_1$	$P2_12_12_1$	$P2_12_12_1$	$P2_12_12_1$
Cell dimensions (a,b,c)	55.30, 52.78, 79.78	55.28, 52.76, 79.67	54.98, 52.67, 79.68	55.09, 52.59, 79.40	55.62, 52.63, 79.53
Resolution range (Å)	40–2.2	40–2.0	50–2.0	40–1.84	50–1.85
Total reflections	48,181	86,588	130,245	164,339	189,986
Unique reflections	11,611	16,421	15,917	21,751	20,041
Completeness (%)					
overall (final shell)	93.2 (96.7)	99.5 (99.1)	99.0 (100.0)	97.9 (99.0)	96.5 (94.4)
R_{merge}† (final shell)	6.2 (27.4)	12.9 (37.1)	5.2 (18.1)	13.8 (48.1)	5.0 (19.4)
R factor‡ (R_{free}§)	20.6 (29.9)	22.2 (28.3)	21.2 (27.9)	20.5 (24.4)	22.2 (28.4)
Rms deviations from ideality#					
bonds (Å)	0.025	0.021	0.028	0.028	0.023
angles (°)	2.83	3.07	2.13	2.92	2.71
Average B factors¶ ($Å^2$)					
protein	12.02	9.75	13.93	12.23	13.46
solvent	13.69	16.52	19.72	21.13	17.20
sulfate	25.91	26.66	30.72	29.95	29.78
inhibitor	5.43	9.73	9.304	10.05	7.39

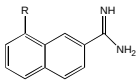

*The substituent R is given at the top of the table. †$R_{sym} = \Sigma ((I - <I>) ** 2) / \Sigma (I ** 2)$. ‡$R_{factor} = \Sigma |F_o - F_c| / \Sigma |F_o|$. §Value of the R factor where 10% of the data were randomly removed from the refinement. #Values were calculated using the parhcskx.pro parameters [56] in X-PLOR. ¶Average B factor is for atoms visible in the electron-density maps.

2-naphthamidine might access $S_{1\beta}$ (Figure 2a). As naphthamidine appears more optimally situated to access additional subpockets near the substrate binding groove in addition to $S_{1\beta}$, 2-napthamidine was chosen as the lead scaffold over benzo(b)thiophene-2-carboxamidine.

The 8-position of 2-naphthamidine was chosen as the initial site for optimization because interactions at the $S_{1\beta}$ pocket have been demonstrated to confer an increased potency in the benzo(b)thiophene-2-carboxamidine series. Can this boost in potency be obtained in a naphthamidine inhibitor by a transfer of functionality? An overlay of B428 and 2-napthamidine shows that the substitution vector of the 8-position of 2-napthamidine is different from that of the 4-position of benzo(b)thiophene-2-carboxamidine, thus suggesting that a direct transfer of functionality might not work (Figure 2a). Given that the iodo-group of B428 interacts with a bridge between S_1 and $S_{1\beta}$, it is also likely that increased potency is dependent on the specific geometry of the interaction and that this is not available for the 2-naphthamidine. This was supported by the observation that 8-iodo-2-napthamidine bound with nearly the same potency (K_i = 2.7 μM; compound **3** Table 2) as the parent. Thus, it is unlikely that the B428 structure–activity relationships at the $S_{1\beta}$ pocket can translate to the 2-naphthamidines.

The $S_{1\beta}$ pocket is a shallow subsite that has not been widely used for structure-based drug design of other serine protease inhibitors. One inhibitor, terphenylbisamidine, has been shown to access $S_{1\beta}$ in trypsin and to hydrogen bond with Asn143 [46]. Because urokinase has a lysine at position 143, however, this inhibitor's substituent would probably interact unfavorably at the $S_{1\beta}$ site of urokinase. The $S_{1\beta}$ subpocket contains a number of polar groups including Gln192 N Gln192 Nε2(Oε1), Lys143 Nζ, Ser146 Oγ and Ser146 O with Gly216 O, Gly218 N and Gly218 O at the bridge from S_1. Furthermore, an ordered solvent molecule is found to occupy this site and hydrogen bond with Gln192 O/N (3.3 Å), Lys143 Nζ (3.3 Å) and possibly Ser146 O (3.7 Å) (Figure 2b). Consequently, hydrophilic 8-substitutions were synthesized to interact with the $S_{1\beta}$ pocket. One group which conferred a tenfold potency increase was benzylcarbamate (K_i = 0.17 μM; compound **5** Table 2). This substitution contains both hydrophobic and hydrophilic components, and from molecular modeling the group is predicted to be too large to be fully accommodated at $S_{1\beta}$. To understand the specific interactions of benzylcarbamate, a crystal structure was determined at 2.0 Å resolution (Table 1).

The crystal structure of 8-benzylcarbamyl 2-aminonaphthamidine (compound **5**) reveals a number of important binding interactions and suggests a strategy for the next round of the design cycle. The electron-density maps reveal strong density for all atoms of the inhibitor except for the benzyl phenyl (Figure 3a) and show the 8-carbamate bound at $S_{1\beta}$ (Figure 3b). The ordered solvent found at $S_{1\beta}$ is not displaced by the carbamate and is hydrogen bonded with the carbonyl oxygen (2.7 Å) of the inhibitor.

Table 2

Structure-activity relationship (SAR) for substituted naphthamidine.

	R7*	R8*	K_i(μM)
1	—H	—H	5.9
2	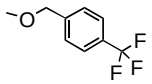	—H	4.8
3	—OCH_3	— I	27
4	—H	—NH_2	0.45
5	—H	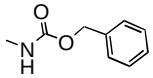	0.17
6	—H		0.04
7	—H		2.2
8	—H		2.1
9	—H	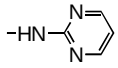	0.03
10	—OCH_3[†]	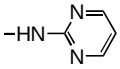	0.05
11	—OCH_3	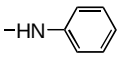	1.7
12	—H	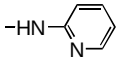	0.17
13	—H	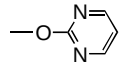	0.55

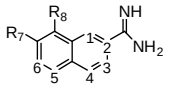

[†]For synthetic reasons, six-membered ring compounds were initially synthesized in the presence of a 7-OCH_3 group.

The carbamyl nitrogen donates a hydrogen bond to Gly216 O (3.4 Å). In addition to these hydrophilic interactions, the carbamyl group is also in van der Waals contact with Gly218, the Cys191–Cys220 disulfide, Gln192 and Ser146, with a close packing interaction between the carbamyl ester oxygen and Gly218 Cα (3.0 Å; Figure 3b). The hydrophobic and hydrophilic interactions between the carbamyl and $S_{1\beta}$ are probably responsible for the binding potency conferred by the benzylcarbamyl group. Conversely, the phenyl group points into the bulk solvent and is disordered in the electron-density map. This disordered group is unlikely, therefore, to contribute to the binding of the 8-benzylcarbamyl compound and in fact, might cost binding energy due to the placing of a hydrophobic group into the bulk solvent.

Because the phenyl group in compound **5** is disordered in the electron density it was removed resulting in the production of 8-methylcarbamyl-2-naphthamidine (compound **6** Table 2). Compound **6** showed a significant increase in inhibitory potency (K_i = 0.04 μM), thus providing one of the most potent nonpeptidic urokinase inhibitor reported to date. The crystal structure of the 8-methylcarbamyl compound (Figure 3c) depicts a hydrogen-bonding geometry for the carbamyl group similar to that of benzyl carbamate in addition to increased hydrophobic packing interactions. Furthermore, removal of the phenyl group of the benzyl substituent allows a rotation about the N–C bond so that the remaining methyl group is closely packed within a hydrophobic dimple. This dimple is composed of Cα and Cβ of Ser146 and Cys220 (Figure 3c). The phenyl group of the benzyl substituent prevents this close interaction and its removal results in more optimal binding at $S_{1\beta}$.

Comparison of the inhibitory potency of 2-napthamidine and 8-methylcarbamyl 2-naphthamidine suggests that hydrophobic and hydrophilic interactions from the methylcarbamyl contribute about 100-fold to the K_i or approximately 3 kcal of binding energy relative to the naphthamidine parent. The ability to accurately predict binding energies computationally has been a difficult task given the contributions of numerous variables such as desolvation, inhibitor structure re-organization and the series of ligand–protein interactions [47]. To estimate the energetic contribution of the individual groups, a series of control compounds was synthesized and assayed. The numbers are simple approximations that are meant to provide a foundation for future design exercises and not intended to address the complex energetic nature of the binding event. The first interaction studied was the carbamate-NH via synthesis of 8-amino-2-naphthamidine (compound **4** Table 2). Compound **4** inhibits urokinase with a K_i of 0.45 μM (Table 2) showing a tenfold increase over the naphthamidine parent (approximately 1.5 kcal). A co-crystal structure of the 8-amino compound, **4** (not shown, data in Table 1) in complex with urokinase was shown to reveal a binding orientation nearly identical to that of the methyl carbamate, where the 8-amino might donate a long hydrogen bond to Gly216 O (distance = 3.7 Å). In addition, the potential for an additional long hydrogen bond to Gly218 O exists (3.4 Å). The geometry for this hydrogen bond is unfavorable for the carbamate compounds. In addition to the potential hydrogen-bonding interactions, it is possible that van der Waals packing between the 8-NH and the entrance to $S_{1\beta}$ might also contribute binding energy, as proposed for the iodine of B428. Nevertheless, it is likely that this group is important for the binding energetics of the 8-carbamyl compounds and that it could contribute up to approximately 1.5 kcal of binding energy.

If the 8-amino group is responsible for 1.5 kcal of binding energy, then the remaining 1.5 kcal of binding energy

Figure 3

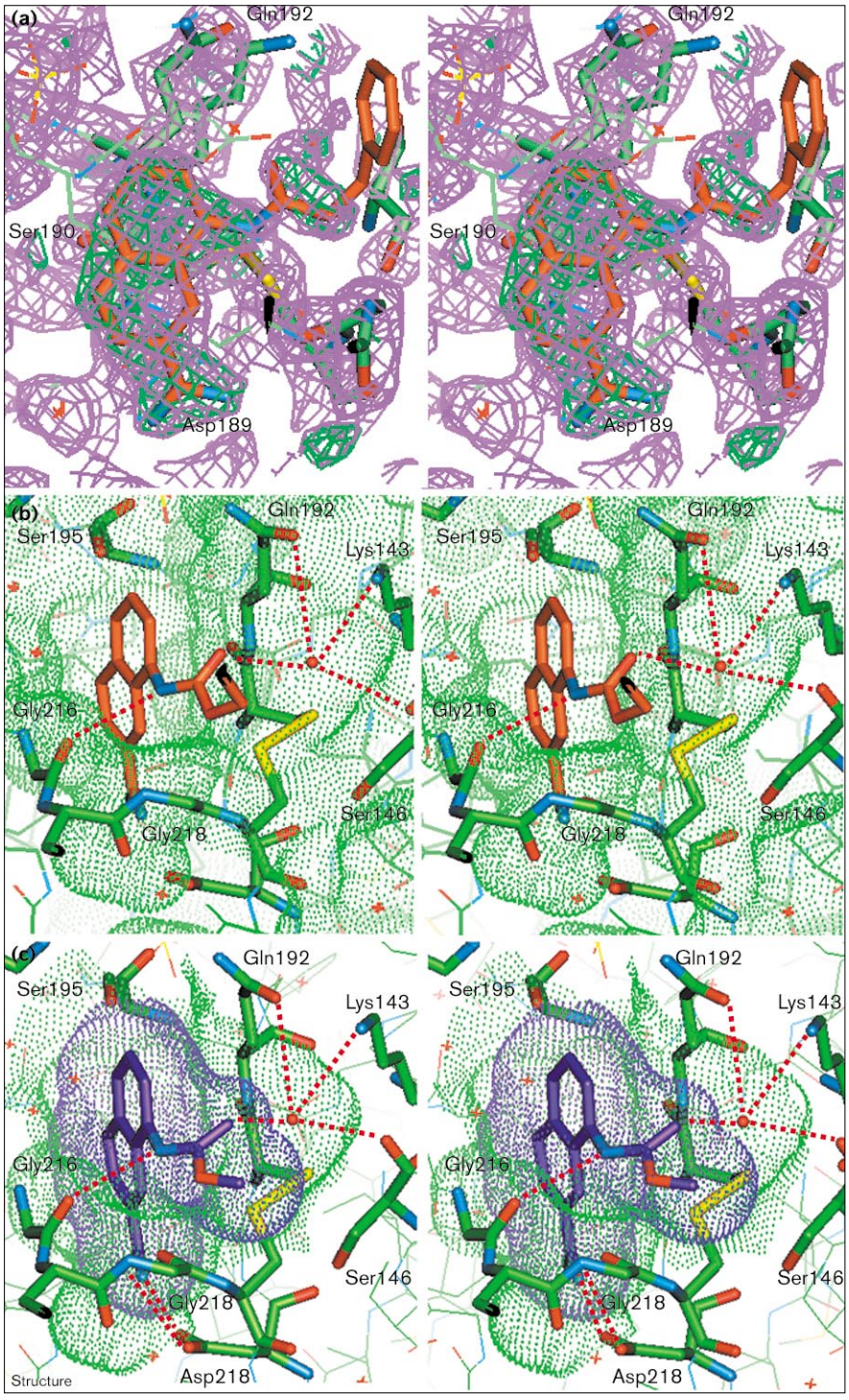

Crystal structures of 8-napthamidines that access $S_{1\beta}$. **(a)** Stereo depiction of the initial $2F_o–F_c$ (1σ, purple) and $F_o–F_c$ (2.5σ, green) maps for the co-crystal structure of 8-benzylcarbamyl-2-napthamidine urokinase at 2.0 Å resolution. Electron density was not present for the benzyl group but was continuous for the rest of the inhibitor. **(b)** Stereo depiction of the binding of 8-benzylcarbamyl-2-napthamidine to urokinase showing hydrogen bonds (red dashed lines) between the carbamate nitrogen and Gly216 as well as the carbamate oxygen and an ordered solvent molecule at $S_{1\beta}$. The Connolly surface for urokinase is depicted in green. **(c)** Stereo diagram depicting the interaction surface and hydrogen bonding between 8-methylcarbamyl-2-napthamidine (dark blue) and urokinase (green). Hydrogen bonds are depicted in red. Atoms are in standard colors.

should arise from the rest of the 8-methyl carbamate. Comparison of the methyl and benzyl carbamate structures shows that the carbamate portion of each molecule makes similar interactions, but that the benzyl methylene interacts less closely with $S_{1\beta}$. The potency difference between the 8-amino (compound **4**) and 8-benzylcarbamyl (compound **5**) suggests an energetic contribution by the carbamyl carbonyl. As discussed above, the carbamyl carbonyl hydrogen bonds with an ordered solvent and the ester oxygen in close contact with Gly218

Figure 4

Structure-based optimization of the 8-position substituent. (a) Design concept based upon the crystal structure of 8-methylcarbamyl 2-naphthamidine showing the feasibility of incorporating a six-membered aromatic ring at this site (depicted as orange dashed lines). The predicted surface interaction (orange for inhibitor and colored by atom type for the protein) shows a complementary lock-and-key fit which would be predicted to confer an increase in binding potency. (b) van der Waals representation of the crystal structure of 8-amino-pyrimidyl-2-naphthamidine showing binding of the pyrimidyl ring as predicted by the design concept (shown as dotted surface). (c) Overlay of the co-crystal structures of the 8-methylcarbamyl (purple) and 8-amino-pyrimidyl (orange) compounds bound to urokinase. The ordered solvent molecule is displaced in the 8-amino-pyrimidyl compound.

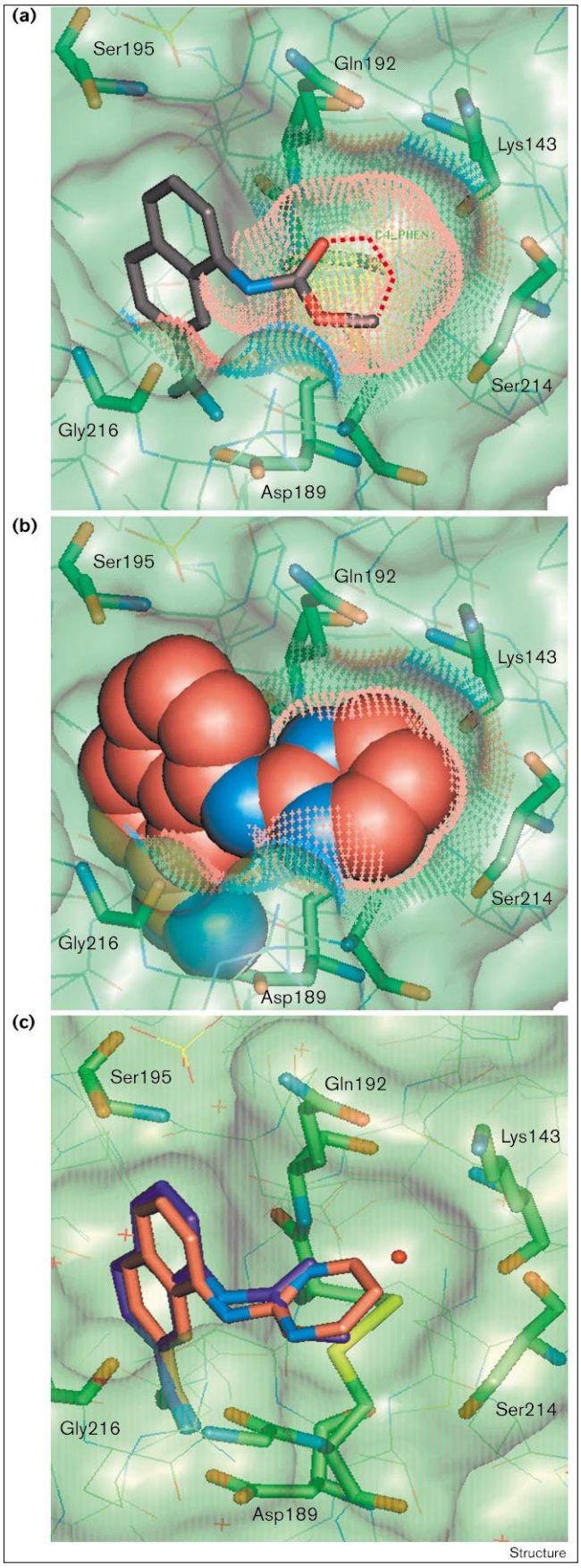

Cα. The ester oxygen interaction was probed through the synthesis and testing of 8-methyl urea (compound **8** Table 2) and 8-ethyl amide (compound **7** Table 2) compounds. Each compound showed decreased potency (K_i of 2.1 μM and 2.2 μM, respectively) relative to the methyl carbamyl compound (compound **6**), thus suggesting subtle interactions at the ester oxygen site. For compounds **7** and **8**, modeling predicts that the hydrogen atoms would interfere with the close packing observed for the ester oxygen, thereby reducing the inhibitory potency. A significant portion of the methyl carbamate binding energy appears to be due to the terminal methyl group, as estimated by comparing potencies of the 8-benzyl carbamate, compound **5**, (where the methyl packing interaction is sterically occluded) and the 8-methyl compound **6**. This energy boost might be estimated assuming that the disordered phenyl group is not negatively effecting the binding energy of compound **5**. The consistent binding of the naphthamidine scaffold for these analogs allows assignment of approximate energetic contributions that provide an experimentally derived map of the binding sites useful for future drug design cycles.

Redesign of the 8-substituent to change chemical properties but maintain potency

Breaking down the energetic contributions of the methyl carbamate and examination of its co-crystal structure provides a template for the design of other $S_{1\beta}$ pocket-directed substituents. These substituents can provide compounds with improved potency, *in vivo* properties, and/or selectivity. The previous analysis demonstrated that the carbamate nitrogen is important for improved binding and that traditional medicinal chemistry isosteric substitutes will not work (urea or ethyl amide). Examination of the carbamate structure suggests that a six-membered aromatic ring would fit the carbamate structure and better complement the $S_{1\beta}$ site (Figure 4a). This led to the synthesis of a series of 8-*N*-linked six-membered ring naphthamidines. Of the rings tested, an 8-aminopyrimidine compound was the most potent inhibitor (K_i = 0.03 μM, compound **9** Table 2). In order to confirm the design concept, a co-crystal structure of

8-aminopyrimidyl naphthamidine was completed, and the structure shows that the pyrimidyl fully occupies $S_{1\beta}$ (Figure 4b) and overlays well with the methyl carbamate structure (Figure 4c). Hence, a second chemically novel substituent that accesses the $S_{1\beta}$ pocket and maintains high binding potency was discovered.

Several six-membered ring analogs (compounds **9–12** Table 2) were prepared to analyze the energetic contributions of the 8-aminopyridyl compound and to contrast with the energetic analysis of the 8-methyl carbamate. The 8-NH is present in both series of inhibitors and makes nearly identical interactions (Figure 4c) with the protein. Furthermore, substitution of the 8-NH linker with an ester (compound **13** Table 2) resulted in a tenfold loss of potency supporting the energetic mapping of the 8-NH interactions using compound **4**. Because the 8-NH-pyrimidyl (compound **9**) and methyl carbamate compounds (**6**) bind with similar affinities, the pyrimidyl ring and methyl carbamate –COOMe are likely to contribute approximately the same amount of binding energy (~1.5 kcal) even though their chemical structures are very different. The structural differences are manifested in the co-crystal structures where the pyrimidyl group occupies more of the $S_{1\beta}$ pocket than the methyl carbamate and displaces the ordered solvent molecule that hydrogen bonds with the carbamate carbonyl. The interaction of the pyrimidyl group might represent a lock-and-key fit, traditionally predicted to confer an increase in binding potency [48]. This is in contrast to the methyl carbamate where binding energy appears to arise from hydrophobic and hydrophilic interactions, including the interaction of the carbamate methyl at the Ser214 dimple that is also disrupted in the pyrimidyl compound. Hence, although the 8-NH interaction of compounds **6** and **9** appears to be both energetically and structurally similar, the overall binding interaction for the remainder of the two $S_{1\beta}$ groups is different.

Although binding of the pyrimidyl and methyl carbamate ester groups appears to be driven by different interactions, they share some common characteristics. One of the pyrimidyl nitrogens occupies the same site as the carbamate ester oxygen and, as observed for the carbamate series, the addition of a hydrogen atom, such as in compound **11**, at this site results in a decrease in binding energy (compounds **7–8** and **11–12** Table 2). This might arise because both the 8-phenyl (**11**, K_i = 1.7 μM) and the 8-pyridyl (**12**, K_i = 0.17 μM) compounds could place a hydrogen atom at the carbamate oxygen site. The phenyl compound is the weakest inhibitor in the six-membered ring series (naphthamidines **9–12** Table 2), and the pyridyl is intermediate between the phenyl and pyrimidyl. The phenyl compound would always place a hydrogen atom at the carbamate oxygen site, whereas the pyrimidyl would have an equally probable chance of placing a hydrogen in the 'less favorable' orientation. In addition, it is possible that a nitrogen would be preferred at both pyrimidyl nitrogen sites as the second nitrogen is approximately 3.7 Å from Gln192 N. At this site a –CH substituent could result in a steric clash or loss of a favorable long range hydrogen-bonding interaction. Hence, although the 8-pyrimidyl and carbamate compounds are chemically different, they appear to share some common packing interactions at $S_{1\beta}$.

Selectivity and the $S_{1\beta}$ pocket

In the development of a clinical agent, selectivity for the target protein is important for reducing the potential for harmful side-effects. This is particularly true for the trypsin-like family of proteases that have been implicated in a number of highly regulated processes including blood coagulation, fibrinolysis and the complement system [49–51]. To monitor selectivity, inhibition of a series of closely related trypsin-like proteases was measured in conjunction with the design process. The naphthamidine lead compound exhibits specificity over plasmin, tissue plasminogen activator and thrombin with limited selectivity over trypsin and kallikrein (Table 3). Addition of the 8-NH functionality confers an increase in potency for all proteins tested. Structurally, this is likely to occur because the 8-NH binding site is highly conserved in all serine proteases. Building the methyl carbamate into $S_{1\beta}$ results in a substantial increase in potency for urokinase, whereas trypsin (and tissue plasminogen activator) gains less. The increase of specificity relative to trypsin, however, was a particular challenge as the naphthamidine parent binds trypsin and urokinase with nearly equal potencies. The $S_{1\beta}$ pocket of bovine trypsin is different from that of urokinase primarily because of an asparagine substitution for Lys143 [52]; filling this site could result in a change of the specificity profile. This region is also conserved in human trypsin [53]. Incorporation of the N-pyrimidyl group, which occupies $S_{1\beta}$ more fully, results in a loss of potency for trypsin while maintaining high potency for urokinase. Hence, binding at $S_{1\beta}$ appears to exploit structural differences between urokinase and trypsin and, thus has resulted in potent and specific urokinase inhibitors.

Two of the most potent nonpeptidic urokinase inhibitors reported to date have been discovered using structure-directed drug design. Naphthamidine served as the starting scaffold and structure-directed optimization began by accessing a novel binding subpocket, termed $S_{1\beta}$, via the 8-position. The two most potent inhibitors (compounds **6** and **9** Table 2) are chemically diverse but share a common hydrogen-bonding interaction estimated to contribute approximately 1.5 kcal of binding energy to each compound. This binding energy was derived from the potency of the control compound 8-amino naphthamidine (compound **4**) and supported by compound **13**. The methyl carbamyl group further interacts at $S_{1\beta}$ through other hydrophilic and hydrophobic interactions. These include

Table 3

Selectivity data for compounds used in this study.

R	–H	$–NH_2$	–NHCOObenz	–NHCOOMe	–NHpyr
Human urokinase	5.9	0.45	0.17	0.04	0.03
Human plasminogen	51	6.6	1.7	1.8	3.8
Human t-PA	100	27	41	40	23
Human kallikrein	22	1.9	1.3	1.5	1
Porcine trypsin	7.8	0.2	0.2	0.3	1.6
Human thrombin	85†	5.2	4.3	5.2	3.9

K_i values are given in μM. t-PA, tissue plasminogen activator. *R, substituents are as described in Table 1. †Published value [57].

hydrogen bonding with an ordered solvent molecule and van der Waals packing of the carbamate ester oxygen and methyl group. In the pyrimidyl compound, the interaction at the carbamate ester oxygen-binding site appears to be preserved, whereas packing of the methyl group is lost. This loss, however, is accompanied by a gain in van der Waals interactions between the 6-membered ring and the $S_{1\beta}$ pocket. Hence, although compounds **6** and **9** access the same binding subsite on urokinase, the chemical diversity of the two substituents gives rise to a variety of binding interactions that yield nearly identical inhibitory potencies. In addition, the diversity of these two substituents results in a filling of $S_{1\beta}$ by the pyrimidyl group that yields selectivity against other serine proteases including trypsin.

The design strategy applied to urokinase relies on interactions at a previously uncharacterized binding subpocket adjacent to the primary substrate-binding site. This strategy was necessary because the substrate-binding pockets typically utilized in structure-directed inhibitor optimization towards other serine proteases [33,38] are blocked by insertion loops in urokinase. Little was known about the functionality and binding interactions required to confer a potency increase at $S_{1\beta}$, and therefore a strategy of structure-directed synthesis was adopted to probe the pocket and begin the drug design process. This led to the discovery of a carbamate series of inhibitors. Further structure-based drug design yielded the pyrimidyl functionality. The initial success with urokinase is encouraging because many important drug targets might lack a large binding site or multiple anchor sites. Hence, this approach can be applied to other drug targets for discovery of more potent and selective inhibitors.

Structure-based drug design and the synthesis of control compounds have permitted an initial energetic mapping of the novel binding subpocket, $S_{1\beta}$, in urokinase. This energetic mapping should contribute to future drug design exercises with urokinase as the *a priori* prediction of binding affinities can be a very difficult task because of the high number of variables that must be considered [48]. Although energetic mapping using X-ray crystal structures and inhibitory potencies is an approximation, the consistency of the results presented here suggests a correlation and implies that the numbers might be applied in future series. This methodology and knowledge, together with the identification of two potent urokinase inhibitors, is being used to further the development of novel, potent and specific small-molecule urokinase inhibitors for the treatment of cancer.

Biological implications

Human urokinase (urokinase-type plasminogen activator, u-PA) has been demonstrated to have a role in the disease progression of cancer. This protein is composed of three domains: the catalytic serine protease domain, a kringle domain and an epidermal growth factor like domain. The C-terminal serine protease domain is responsible for activation of the inactive zymogen, plasminogen, into the active protease, plasmin. Plasmin, in turn, is responsible for the degradation of basement membrane and interstitial proteins that facilitates tumor growth and metastasis. The N-terminal domains serve to anchor urokinase to the membrane surface through a specific urokinase receptor (uPAR) but have not been implicated in the catalytic activity of the enzyme. Hence, urokinase-mediated cancer progression might be blocked at two junctions. Firstly, inhibiting the urokinase–uPAR receptor interaction might indirectly block substrate cleavage by limiting access to the membrane-bound plasminogen. Secondly, urokinase activity might also be directly blocked through inhibition of the catalytic activity of the serine protease domain. To effect this second strategy, structure-based drug design has been used to discover two novel, potent and specific urokinase inhibitors.

The discovery of novel urokinase inhibitors using structure-based drug design has been expedited through use of a new crystal form of human urokinase. This crystal form arises from a re-engineered urokinase that has been shown to possess catalytic properties similar to the native enzyme. The re-engineered protein lacks the N-terminal domain, yields more efficient crystal packing resulting in higher resolution structures, and permits formation of crystalline complexes using the method of compound soaking. Use of this crystal system has permitted structural characterization of a novel binding subsite

adjacent to the primary binding pocket and substrate-binding groove, yielding two new urokinase inhibitors. These compounds are the most potent urokinase inhibitors reported to date, and this information is being used to expedite discovery of an anticancer clinical agent.

Materials and methods

Amidolytic kinetics of urokinase and microurokinase

The effect of synthetic inhibitors on the steady-state amidolytic activity of urokinase was completed as described [34]. Specifically, synthetic compounds were tested for inhibitory activity against urokinase (2–3 nM; S-2444, pyroGlu-Arg-pNA-HCl, 200 μM), human plasma kallikrein (100 ng ml^{-1}, S-2302, H-D-Pro-Phe-Arg-pNA-2HCl, 330 μM), human plasmin (18 nM, S-2251, H-D-Val-Leu-Lys-pNA-2HCl, 360 μM), human α-thrombin (8 nM, S-2302, H-D-Pro-Phe-Arg-pNA-2HCl, 820 μM), human t-PA (1 μg ml^{-1}, S-2288, H-D-Ile-Pro-Arg-pNA-2HCl, 1350 μM) and porcine trypsin (1.25 nM; S-2444, pyroGlu-Arg-pNA-HCl, 200 μM). Chromogenic substrates were obtained from DiaPharma Group, Inc. Distributor of Chromogenix. All enzymes were obtained from commercial sources (kallikrein, t-PA, and trypsin, Sigma; plasmin, DiaPharma; thrombin, Enzyme Research Laboratories; human urokinase, Abbokinase, Abbott Laboratories). The assay was performed in a 96-well polystyrene, flat-bottom plate in a 50 mM Tris/0.15 M NaCl and 0.5% Pluronic F-68 (Σ P-5556), pH 7.4 (with HCl) buffer. The compounds were dissolved in dimethylsulfoxide (DMSO), and tested at 0.01–250 μM concentrations in a final reaction volume of 200 μl. The reactions were initiated by the addition of substrate, and were followed by the formation of *p*-nitroanaline at 405 nm at 25°C on a Spectromax (Molecular Devices) plate reader for 15 min. K_i values were calculated from the percent inhibition and previously established K_m values.

Protein crystallography

Protein was prepared and crystallized as reported previously [34]. Complex structures were obtained by the soaking method using DMSO as the co-solvent [34] and the solid compound was obtained from the Abbott chemical repository. Details for the synthesis of these compounds will be presented elsewhere. Data were collected at 160K as described [34] and processed using the HKL program suite [54]. Initial electron-density maps were calculated and complexes refined using the program package X-PLOR [55]. All electron-density maps were inspected on a Silicon Graphics INDIGO2 workstation using QUANTA 97, and the orientation of all compounds were clearly visualized in the initial $2F_o–F_c$ map. Ordered solvent molecules were identified as positive peaks in the $F_o–F_c$ map that were 4σ above noise. All data were of high quality to the highest resolution shell and well refined as summarized in Table 1.

Acknowledgements

The authors would like to thank Jonathan Greer for helpful discussions and for critical evaluation of this manuscript.

References

1. Behrendt, N., Ronne, E., Ploug, M., Petri, T. & Lober, D. (1990). The human receptor for urokinase plasminogen activator. NH2-terminal amino acid sequence and glycosylation variants. *J. Biol. Chem.* 265, 6453-6460.
2. Schmitt, M., Janicke, F., Moniwa, N., Chucholowski, N. & Pache. (1992). Tumor-associated urokinase-type plasminogen activator: biological and clinical significance. *Biol. Chem. Hoppe Seyler* 373, 611-622.
3. Duffy, M.J. (1990). Plasminogen activators and cancer. *Blood Coagul. Fibrinolysis* 1, 681-687.
4. Busso, N., Pleclat, V., So, A. & Sappino, A.-P. (1997). Plasminogen activation in synovial tissues: differences between normal, osteoarthritis, and rheumatoid arthritis joints. *Ann. Rheum. Dis.* 56, 550-557.
5. Ronday, H.K., *et al.*, & Verheijen J.H. (1997). Bone matrix degradation by the Plasminogen activation system. Possible mechanism of bone destruction in arthritis. *Br. J. Rheumatol.* 36, 9-15.
6. Carmeliet, P. *et al.*, & Collen, D. (1997). Urokinase-generated plasmin activates matrix metalloproteinases during aneurysm formation. *Nat. Genet.* 17, 439-444.
7. Noda-Heiny, H., Daugherty, A. & Sobel, B.E. (1995). Augmented urokinase receptor expression in atheroma. *Arterioscler. Thromb. Vasc. Biol.* 15, 37-43.
8. Heymans, S., *et al.*, & Carmeliet, P. (1999). Inhibition of plasminogen activators or matrix metalloproteinases prevents cardiac rupture but impairs therapeutic angiogenesis and causes cardiac failure. *Nat. Med.* 5, 1135-1142.
9. Kohn, E.C. (1991). Invasion and metastasis: biology and clinical potential. *Pharmacol. Ther.* 52, 235-244.
10. Reuning, U., *et al.,* & Schmitt, M. (1998). Multifunctional potential of the plasminigen activation system in tumor invasion and metastasis. *Int. J. Oncol.* 13, 896-906.
11. Shapiro, R.L., *et al.*, & Rifkin, D.B. (1996). Induction of primary cutaneous melanocytic neoplasms in urokinase-type plasminogen activator (uPA)-deficient and wild-type mice: cellular blue nevi invade but do not progress to malignant melanoma in uPA-deficient animals. *Cancer Res.* 56, 3597-3604.
12. Evans, D., Sloan-Stakleff, K., Arvan, M. & Guyton, D. (1998). Time and dose dependency of the suppression of pulmonary metastasis of rat mammary cancer by amiloride. *Clin. Exp. Metastasis* 16, 353-357.
13. Banerji, A., Fernandes, A., Bane, S. & Ahire, S. (1998). The field bean protease inhibitor has the potential to suppress B16F10 melanoma cell lung metastasis in mice. *Cancer Lett.* 129, 15-20.
14. Rabbani, S., Harakidas, P., Davidson, D., Henkin, J. & Mazar, A. (1995). Prevention of prostate-cancer metastasis *in vivo* by a novel synthetic inhibitor of urokinase-type plasminogen activator. *Int. J. Cancer* 63, 840-845.
15. Alonso, D.F., Tejera, A.M., Farias, E.F., Bal de Kier Joffe, E. & Bomez, D.E. (1998). Inhibition of mammary tumor cell adhesion, migration, and invasion by the selective synthetic urokinase inhibitor B428. *Anticancer Res.* 18, 4499-4504.
16. Alonso, D., *et al.*, & Bal de Kier Joffe, E. (1996). Effects of synthetic urokinase inhibitors on local invasion and metastasis in a murine mammary tumor model. *Breast Cancer Res. Treat.* 40, 209-223.
17. Tressler, R.J., *et al.*, & Rosenberg, S. (1999). Urokinase receptor antagonists: discovery and application to *in vivo* models of tumor growth. *APMIS* 107, 168-173.
18. Ignar, D.M., *et al.*, & Emerson, D.L. (1998). Inhibition of establishment of primary and micrometastatic tumors by a urokinase plasminogen activator receptor antagonist. *Clin. Exp. Metastasis* 16, 9-20.
19. Mueller, B.M., Yu, Y.B. & Laug, W.E. (1995). Overexpression of plasminogen activator inhibitor 2 in human melanoma cells inhibits spontaneous metastasis in scid/scid mice. *Proc. Natl Acad. Sci. USA* 92, 205-209.
20. Foekens, J.A., *et al.*, & Kramer, M.D. (1995). Plasminogen activator inhibitor-2: prognostic relevance in 1012 patients with primary breast cancer. *Cancer Res.* 55, 1423-1427.
21. Fleisher, M. (1998). Prognostic markers other than hormone receptors in breast cancer. *J. Clin. Ligand Assay* 21, 41-46.
22. Grondahl-Hansen, J., *et al.*, & Brunner, N. (1997). Plasminogen activator inhibitor type 1 in cytosolic tumor extracts predicts prognosis in low-risk breast cancer patients. *Clin. Cancer Res.* 3, 233-239.
23. Bajou, K., *et al.*, & Foidart, J.M. (1998). Absence of host plasminogen activator inhibitor 1 prevents cancer invasion and vascularization. *Nat. Med.* 4, 923-928.
24. Kim, S.J., *et al.*, & Takai, S. (1998). Prognostic impact of urokinase-type plasminogen activator (PA), PA inhibitor type-1 and tissue-type PA antigen levels in node-negative breast cancer: a prospective study on multicenter bases. *Clin. Cancer Res.* 4, 177-182.
25. Harbeck, N., *et al.*, & Schmitt, M. (1998). Prognostic impact of tumor biological factors on survival in node-negative breast cancer. *Anticancer Res.* 18, 2187-2197.
26. Ke, S.H., Coombs, G.S., Tachias, K., Corey, D.R. & Madison, E.L. (1997). Optimal subsite occupancy and design of a selective inhibitor of urokinase. *J. Biol. Chem.* 272, 20456-20462.
27. Spraggon, G., *et al.*, & Jones, E.Y. (1995). The crystal structure of the catalytic domain of human urokinase-type plasminogen activator. *Structure* 3, 681-691.
28. Tidwell, R., Geratz, J. & Dubovi, E. (1983). Aromatic amidines: comparison of their ability to block respiratory syncytial virus induced cell fusion and to inhibit plasmin, urokinase, thrombin, and trypsin. *J. Med. Chem.* 26, 294-298.
29. Towle, M.J., *et al.*, & Littlefield, B. A. (1993). Inhibition of urokinase by 4-substituted benzo(b)thiophene-2-carboxamidines: an important new class of selective low molecular weight urokinase inhibitor. *Cancer Res.* 53, 2553-2559.

30. Bridges, A.J., Lee, A., Schwartz, C.E., Towle, M.J. & Littlefield, B.A. (1993). The synthesis of three 4-substituted benzo[b]thiophene-2-carboxamidines as potent and selective inhibitors of urokinase. *Bioorg. Med. Chem.* **1**, 403-410.
31. Sturzebecher, J. & Markwardt, F. (1978). Synthetische Inhibitoren der Serinproteinasen. *Pharmazie* **33**, 599-602.
32. Yang, H., Henkin, J., Kim, K.H. & Greer, J. (1990). Selective inhibition of urokinase by substituted phenylguanidines: quantitative structure-activity relationship analyses. *J. Med. Chem.* **33**, 2956-2961.
33. Renatus, M., Bode, W., Huber, R., Sturzebecher, J. & Stubbs, M. (1998). Structural and functional analyses of benzamidine-based inhibitors in complex with trypsin: implications for the inhibition of factor Xa, t-PA and urokinase. *J. Med. Chem.* **41**, 5445-5456.
34. Nienaber, V., Wang, J., Davidson, D. & Henkin, J. (2000). Re-engineering of human urokinase provides a system for structure-based drug design at high resolution and reveals a novel binding subsite. *J. Biol. Chem.* **275**, 7239-7248.
35. Das, J. & Kimball, S.D. (1995). Thrombin active site inhibitors. *Bioor. Med. Chem.* **3**, 999-1007.
36. Sanderson, P.E. & Naylor-Olsen, A.M. (1998). Thrombin inhibitor design. *Curr. Med. Chem.* **5**, 289-304.
37. Kamata, K., Kawamoto, H., Honma, T., Iwama, T. & Kim, S.H. (1998). Structural basis for chemical inhibition of human blood coagulation. *Proc. Natl Acad. Sci. USA* **9**, 6630-6635.
38. Brandstetter, H. *et al.*, & Engh, R. A. (1996). X-ray structure of active site-inhibited clotting factor Xa. Implications for drug design and substrate recognition. *J. Biol. Chem.* **271**, 29988-29992.
39. Bode, W. & Schwager, P. (1975). The refined crystal structure of bovine beta-trypsin at 1.8 Å resolution. II. Crystallographic refinement, calcium binding site, benzamidine binding site and active site at pH 7.0. *J. Mol. Biol.* **98**, 693-717.
40. Bode, W., Mayr, I., Baumann, U., Huber, R. & Stone, S.R. (1989). The refined 1.9 Å crystal structure of human alpha-thrombin: interaction with D-Phe-Pro-Arg chloromethylketone and significance of the Tyr-Pro-Pro-Trp insertion segment. *EMBO J.* **8**, 3467-3475.
41. Padmanabhan, K., *et al.*, & Huber, R. (1993). Structure of human des(1–45) factor Xa at at 2.2 Å resolution. *J. Mol. Biol.* **232**, 947-966.
42. Renatus, M., *et al.,* & Stubbs, M. (1997). Structural mapping of the active site specificity determinants of human tissue-type plasminogen activator. Implications for the design of low molecular weight substrates and inhibitors. *J. Biol. Chem.* **272**, 21713-21719.
43. Geratz, J.D., Shaver, S. & Tidwell, R.R. (1981). Inhibitory effect of amidino-substituted heterocylic compounds on the amidase activity of plasmin and of high and low molecular weight urokinase and on urokinase-induced plasminogen activation. *Thromb. Res.* **24**, 73-83.
44. Engh, R.A., *et al.*, & von der Saal, W (1996). Enzyme flexibility , solvent and 'weak' interactions characterize thrombin-ligand interactions: implications for drug design. *Structure* **4**, 1353-1362.
45. Stubbs, M., Huber, R. & Bode, W. (1995). Crystal structures of factor Xa specific inhibitors in complex with trypsin: structural grounds for inhibition of factor Xa and selectivity against thrombin. *FEBS Lett.* **375**, 103-107.
46. von der Saal, W., *et al.*, & Sauer, J. (1996). Syntheses and selective inhibitory activities of terphenyl-bisamidines for serine proteases. *Arch. Pharm.* **329**, 73-82.
47. Jackson, R. (1995). Update on computer-aided drug design. *Curr. Opin. Biotechnol.* **6**, 646-651.
48. Verlinde, C.L. & Hol, W.G. (1994). Structure-based drug design: progress, results and challenges. *Structure* **2**, 577-87.
49. Stubbs, M. & Bode, W. (1993). A player of many parts: the spotlight falls on thrombin's structure. *Thromb. Res.* **69**, 1-58.
50. Fevig, J., *et al.*, & Wexler, R (1998). Rational design of boropeptide thrombin inhibitors: β,β-dialkyl-phenethylglycine P2 analogs of DuP 714 with greater selectivity over complement factor I and an improved safety profile. *Bioorg. Med. Chem. Lett.* **8**, 301-306.
51. Collen, D. & Lijnen, H. (1995). Molecular basis of fibrinolysis, as relevant for thrombolytic therapy. *Thromb. Haemost.* **74**, 167-171.
52. Marquart, M., Walter, J., Deisenhofer, J., Bode, W. & Huber, R. (1983). The geometry of the reactive site and of the peptide groups in trypsin, trypsinogen and its complexes with inhibitors. *Acta Crystallogr. B* **39**, 480.
53. Emi, M., *et al.*, & Matsubara, K. (1986). Cloning, characterization and nucleotide sequences of two cDNAs encoding human pancreatic trypsinogens. *Gene* **41**, 305-310.
54. Otwinowski, Z. & Minor, W. (1997). Processing of X-ray diffraction data collected in oscillation mode. *Methods Enzymol.* **276**, 307-326.
55. Brünger, A.T. (1993) *X-PLOR version 3.1 manual*, Yale University Press, New Haven, Conneticut.
56. Engh, R.A. & Huber, R. (1991). Accurate bond and angle parameters for X-ray protein-structure refinement. *Acta Crystallogr. A* **47**, 392-400.
57. Wagner, G., *et al.*, & Walsmann, P. (1977). Synthetic inhibitors of serum proteinases. Part 15: Antitrypsin, antiplasmin, and antithrombin effect of 2-amidino-6-alkoxy- and aralkoxynaphthalenes. *Pharmazie* **32**, 761-763.
58. Nicholls, A., Sharp, K. & Honig, B. (1991). Protein folding and association: insights from interfacial and thermodynamic properties of hydrocarbons. *Proteins* **11**, 281-296.

Because *Structure with Folding & Design* operates a 'Continuous Publication System' for Research Papers, this paper has been published on the internet before being printed (accessed from http://biomednet.com/cbiology/str). For further information, see the explanation on the contents page.